SCIENCE CHINA Materials ARTICLES

mater.scichina.com link.springer.com

Published online 20 July 2020 | https://doi.org/10.1007/s40843-020-1383-3
Sci China Mater 2020, 63(12): 2477–2486

Boosting optoelectronic performance of $MAPbI_3$ perovskite solar cells *via* ethylammonium chloride additive engineering

Muhammad Mateen[1], Zulqarnain Arain[1,3], Xuepeng Liu[1*], Atif Iqbal[1], Yingke Ren[4], Xianfu Zhang[1], Cheng Liu[1], Qin Chen[1], Shuang Ma[1], Yong Ding[1,2*], Molang Cai[1,2] and Songyuan Dai[1,2*]

ABSTRACT **The quality of the perovskite light absorption layer plays a dynamic role in the photovoltaic properties of solar cells. The existing methods to prepare methylammonium lead iodide ($MAPbI_3$) films render substantial structural defect density, particularly at the grain boundaries and film surface, constituting a challenge that hinders the further optoelectronic enhancement of perovskite solar cells. Herein, a unique approach was introduced: using a simple ethylammonium chloride (EACl) additive in perovskite precursor mixture to produce high-quality $MAPbI_3$ thin films. The results indicated that EACl could encourage perovskite crystal growth without experiencing the intermediate phase formation and would evaporate from the perovskite after annealing. Additionally, a gradient perovskite structure was achieved using this technique, which impressively enhanced the performance of the perovskite films. A high power conversion efficiency (PCE) of 20.03% was achieved under the optimal amount of EACl, and the resultant efficient device could retain over 89% of the original PCE after aging for 1000 h at room temperature. This novel technique leads to a facile fabrication of high-quality and less-defect perovskite thin films for competent and stable devices.**

Keywords: perovskite solar cells, ethylammonium chloride, crystal growth, stability

INTRODUCTION

In recent decades, organo-metallic halide perovskite has evolved in the solar energy conversion field as a rising and promising material for the future photovoltaic industry. Certain benefits can be yielded through the robust performance of perovskite solar cells (PSCs), such as long-range charge carrier transportation, flexible optical band gap, and effective absorption of light [1–5]. A rapid boost in power conversion efficiency (PCE) from 3.8% to 25.2% is proof for the success of PSCs [6,7], mainly because of optimized material stoichiometry, solvent engineering, controlled crystal growth, and improved surface engineering [5,8]. The rapidly increased PCE is also attributed to the advancement in interface designs, material engineering, and facile fabrication processes such as vacuum evaporation, sequential deposition technique, vapor-assisted, and additive-assisted deposition [9–15]. Pure perovskite material, based on methylammonium (MAI) cation, with an optical band gap of 1.55–1.6 eV is commonly used as a light-harvesting layer in PSCs [16–18]. It can be produced simply *via* many different techniques, such as one-step and two-step spin coatings, inter-diffusion, sequential dip coating, and many other deposition techniques [10].

However, regardless of the exceptionally enhanced performance, a crucial problem inhibiting further performance enhancement and large-scale reproducibility toward commercialization is perovskite phase reversibility [19]. MAI perovskite holds tetragonal phase symmetry under ideal conditions, but it is stated to experience a reversible phase change between tetragonal and cubic phases under some specified processing conditions, which substantially affects the PSC stability and degrades interfaces under normal working condition [20]. Therefore,

[1] Key Laboratory of Novel Thin-Film Solar Cells, North China Electric Power University, Beijing 102206, China
[2] State Key Laboratory of Alternate Electrical Power System with Renewable Energy Sources, North China Electric Power University, Beijing 102206, China
[3] Energy Systems Engineering Department, Sukkur IBA University, Sukkur 65200, Pakistan
[4] College of Science, Hebei University of Science and Technology, Shijiazhuang 050018, China
[*] Corresponding authors (emails: liuxuepeng@ncepu.edu.cn (Liu X); dingy@ncepu.edu.cn (Ding Y); sydai@ncepu.edu.cn (Dai S))

for additional improvements in long-term stability and large-area PSC devices, phase stability will be a serious concern to be dealt with for practical applications of PSCs [21]. Moreover, surface morphologies and crystallization of perovskite thin films are mainly controlled by nucleation and crystal growth, which are also difficult to control [21,22]. Unprompted defects in the films can degrade the performance of the device and cause instability issues due to energy disorder, thereby moisturizing the exposed invasion sites and minimizing concentrations of the charge carriers [22]. Thus, we must increase the performance and extend the stability of PSCs by reducing the flaws in perovskite crystal growth. To control the crystallization and improve the phase stability of perovskite, several methods have been applied, such as additive engineering, composition modulation, and solvent engineering [23,24]. Additive engineering has been reported to offer a positive impact on perovskite thin-film synthesis by regulating crystal evolution (for example by inducing homogeneity through more uniform crystal nucleation) and moderating crystallinity (through retarded crystallization and change in the surficial energy) [25].

Additive engineering is an easy and reproducible technique that can improve the morphology of perovskite films [26]. To coordinate with the perovskite precursor, many additives like acetonitrile, thiourea, and dimethyl sulfoxide (DMSO) are used to formulate the intermediate phase. These additives can intervene with the growth process of perovskite crystal through different methods and reduce the grain boundaries and defects [27]. Perovskite film processed *via* additive engineering concepts is frequently reported to change the morphological patterns of nucleation dynamics [28–30]. Lee *et al.* [31] utilized DMSO to form transitional adducts with PbI_2 to gain high-quality thin films with high photovoltaic presentation. Liang *et al.* [12] investigated 1,8-di-iodo octane additive-accelerated crystallization and moderated the kinetic growth of seed crystals during nucleation to achieve smooth perovskite morphology. Bi *et al.* [19] suggested mixing H_2O in a perovskite precursor to fabricate high-quality perovskite film. Perovskite films with minimal trap states and large grains were produced because of morphological linearity [32]. The drawbacks of perovskite films are still not limited essentially due to the high additive diffusion into the active layer that can lead to undesired interfacial consequences, such as charge carrier leakages into anti-selective layers. In this regard, finding more chemically sound additives to boost perovskite nucleation for producing high-quality perovskite thin films with substantial grain size, low trap density, and suitability for commercial fabrication, but without negotiating the film morphology and band gap, is highly necessary [18].

Here, our work presents a unique and facile additive engineering approach to offer control over perovskite film morphology and crystal quality, as well as scalability for other applications. Introducing ethylammonium chloride (EACl) as an additive in the perovskite precursor solution casted a high-quality perovskite thin film with large crystal size and improved crystallization, resulting in decent carrier lifetime and enhanced material conductivity. This large cation additive incorporation technique is proved to be effective in tuning the perovskite film quality without compromising the band gap of the material. The improvement in morphology due to film passivation considerably reduced the trap density, repressing non-radiative recombination and prolonging charge carrier lifetime. The improved morphology boosted the PCE from 17.35% to 20.03% after introducing the optimal concentration of EACl. The optimized devices also exhibited superior stability.

EXPERIMENTAL SECTION

The detailed materials, characterizations, and device fabrication are illustrated in the Supplementary information. To obtain $MAPbI_3$ thin films with a smooth morphology and optimally sized crystals, varied amounts (mol% relative to stoichiometric $MAPbI_3$) of EACl were doped to prepare the perovskite precursor solution and traditionally spin-coated onto the conductive substrate *via* an orthodox simple one-step method. For the EACl-engineered perovskite precursor, different amounts of EACl (0%, 1%, 2.5%, and 3.5% molar ratios) were added to the pure perovskite precursor. The solution was then heated at 60°C for 1 h under stirring. A perovskite precursor solution containing MAI, EACl, and PbI_2 was mixed into DMSO, and the *N*,*N*-dimethylformamide (DMF)-based solvent system (40 μL) was spin-coated on the meso-TiO_2 substrate at 1100 and 4500 r min^{-1} for 10 and 30 s, respectively. During the second stage of spin coating, 120 μL of anhydrous chlorobenzene (CB) was slowly dripped on the center of the rotating film in the last 10 s during the process. The deposited films were sequentially annealed to an initial temperature of 70°C, at which the film color spontaneously turned into dark brown, and then further annealed at 150°C for 30 min, during which the film completely turned into a black $MAPbI_3$ perovskite.

For convenience in expression, the films were labeled as

EACl-0% (control), EACl-1%, EACl-2.5%, and EACl-3.5%, where 1, 2.5, and 3.5 represent the different mol% percentages of EACl added into the precursor solution.

RESULTS AND DISCUSSION

The molecular structures of MA^+ and EA^+ are displayed in Fig. 1b. Fig. 1a schematically illustrates the step-by-step perovskite film synthesis *via* the EACl doping method, which was illustrated in the EXPERIMENTAL SECTION. The morphological structure of the doped films with different EACl concentrations was examined by scanning electron microscopy (SEM) images. Fig. 1c–f show the top-views of the perovskite films without EACl and with different amounts of EACl additive. The EACl-0% film consisted of fine crystals with an average grain size, which is not favorable for ideal charge transport and collection due to large grain boundaries [33]. The introduction of EACl triggers a visible increase in the grain size of the perovskite film and the film morphology becomes more homogeneous with the increase in the EACl concentration from 1% to 3.5% in the films (Fig. S1). The EACl-2.5% film was more uniform with fewer grain boundaries among all the doped films. This crystal size improvement was supported by previously reported studies, where EACl was also found to boost the surge in grain size and reduce the lattice disorder [33,34].

To determine the effect of EACl on the film quality, atomic force microscopy (AFM) was conducted. The film roughness was measured by calculating the root mean square (RMS) of the prepared films. The control film was composed of small grains with an RMS roughness of 22.4 nm. The RMS gradually decreased to 18.3 nm for EACl-1%, 17.1 nm for EACl-2.5%, and rose to 21.8 nm for EACl-3.5%, as shown in Fig. S2. The witnessed smoothness and uniformity at micro-scale confirmed that the EACl-2.5%-doped film showed more homogeneity and smoothness compared with the other doped films [18].

X-ray diffraction (XRD) was conducted to study the role of EACl in the crystal dynamics of the perovskite films (Fig. 2a). The crystallinity of the films prepared by using EACl was generally enhanced with increasing dopant concentration until it reached EACl-2.5%. Although an excessive amount of EACl-3.5% faintly reduced the crystallinity, no extra peak appeared, suggesting the absence of a second phase [35]. The peak intensity of the EACl-2.5% perovskite was also stronger than that of the other films. By using this method, the crystallization of the films was enhanced [36]. The presence of this possible intermediate phase somehow slowed down nucleation and led to enhanced crystallinity in the final films, which was consistent with the SEM measurements.

Fig. 2b shows the ultraviolet-visible (UV-Vis) absorption spectra of the prepared $MAPbI_3$ films doped with different EACl concentrations. The absorbance of the projected light by the EACl-doped films generally remained noticeably higher than that of the EACl-0% film. Among all the treated films, the EACl-2.5% film exhibited stronger spectral absorbance throughout the UV-Vis spectrum, thereby supporting the morphological claims

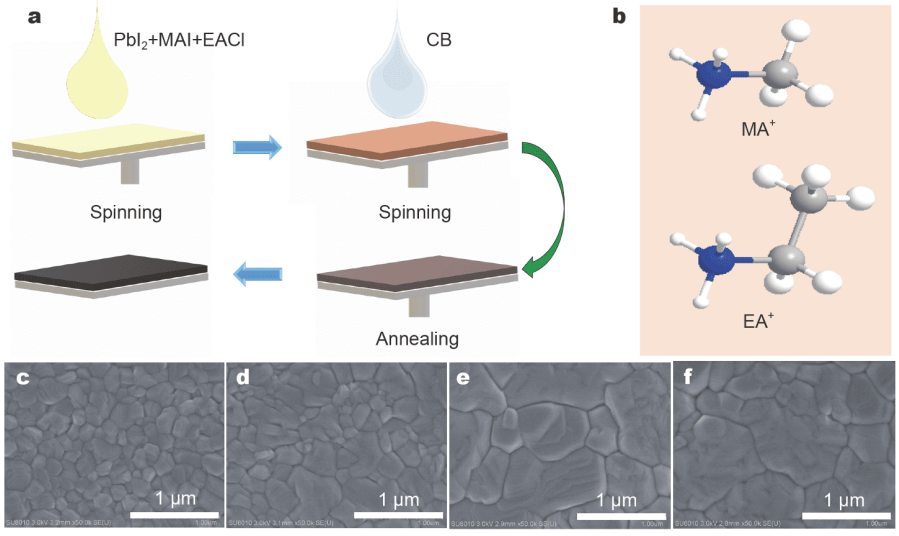

Figure 1 (a) Schematic illustration of the high-quality perovskite film fabrication process employing EACl in precursor solution. (b) Molecular structures of MA and EA. Top-view SEM images of $MAPbI_3$ films with different EACl concentrations: (c) control film (EACl-0), (d) EACl-1%, (e) EACl-2.5%, and (f) EACl-3.5%.

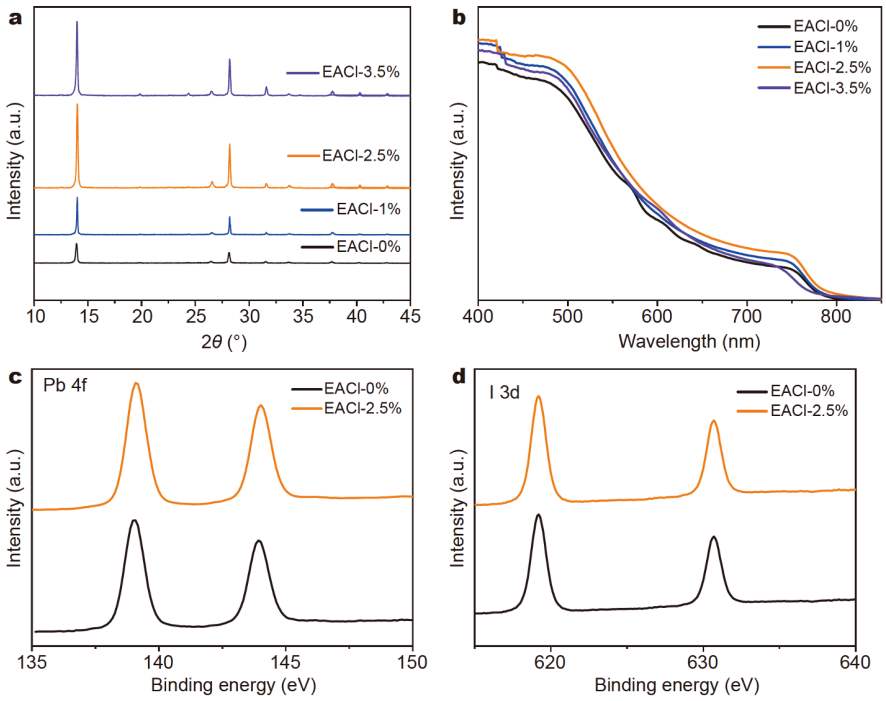

Figure 2 (a) XRD of the $MAPbI_3$ perovskite films engineered with different EACl additive concentrations and (b) UV-Vis spectra of the films without and with EACl additive. XPS of EACl-0%- and EACl-2.5%-doped films: (c) Pb 4f and (d) I 3d core spectra.

of large and compact grain morphology. The high absorbance intensity in both low and high wavelength regions could be credited to the aligned and rigid crystal lattice structure, which was the result of controlled seed crystal evolution induced by the EACl additive. No obvious band edge shift in the UV-Vis spectra was observed as the EACl concentration increased, signifying that the incorporated larger size cation EA amount in the crystal lattice was infrequent [37]. Given that the enlargement of cubic octahedral volume also led to the change in chemical bonding between Pb and I, we further discovered the effect of EACl on the chemical composition of the control and EACl-2.5% by conducting X-ray photoelectron spectroscopy (XPS), as shown in Fig. 2c, d and Fig. S3. The binding energies of Pb 4f and I 3d did not shift with the increased EACl-2.5% content in the doped film. The Pb 4f and I 3d peak intensities of the EACl-2.5% film remained higher than those of the EACl-0% film. All of these observations indicated that most of the volatile EACl was evaporated during the annealing stage [15,37,38].

On the basis of the above crystallographic and morphological analyses, we proposed a credible notion regarding the intermediate transitional mechanism for the synthesis of high-quality MAI-based film with large grain size and low defect crystallinity, as illustrated in Fig. 3. EACl treatment induced an ion exchange process in MAI-EACl-PbI_2-DMSO, thereby suppressing the nucleation rate and allowing grains more time to grow and self-embed into the lattice network [39,40].

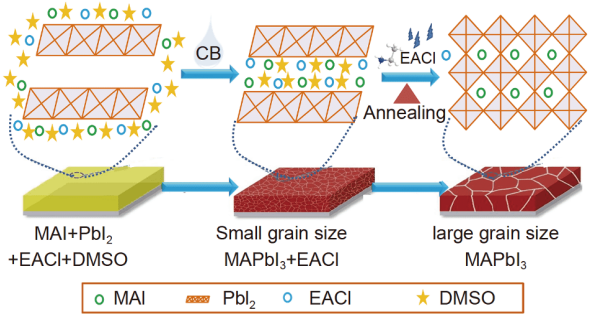

Figure 3 Schematic illustration of the MAI-PbI_2-EACl precursor for the formation of grain and highly crystalline $MAPbI_3$ perovskite film.

All these findings suggested that EACl could encourage perovskite grain growth in a way different from all the earlier reported studies, demonstrating EACl as a potential additive in modifying the quality of perovskite thin films for efficient and large-scale perovskite cell fabrication. Fig. 3 illustrates the proposed mechanism of EACl

additive-based large grain $MAPbI_3$ perovskite thin films.

To analyze the trap density of the prepared films, photophysical measurements were performed for the control (without EACl) and EACl-2.5%-based films. Steady-state photoluminescence (PL) and time-resolved PL (TRPL) were carried out to explore the trap states in the fabricated perovskite bulk (Fig. 4). The studied films were fabricated on the bare glass side of the fluorine-doped tin oxide (FTO). The PL intensity shown in Fig. 4a demonstrated that the EACl-2.5% film presented a much stronger and higher PL intensity than the EACl-0% film. The EACl-2.5% film exhibited a stronger peak than the EACl-0% film, showing the defects at the film surface were reduced. The TRPL decay curve was fitted by double exponential function to calculate the carrier lifetime (τ_{ave}), as follows [39]:

$$f(t) = \sum_i A_i \exp\left(-\frac{t}{\tau_i}\right) + f_0, \quad (1)$$

$$\tau_{ave} = \frac{\sum A_i \tau_i^2}{\sum A_i \tau_i}. \quad (2)$$

The observed decays were analyzed by a bi-exponential model with a fast and a slow component and the extracted lifetime parameters. The EACl additive film yielded a slow fluorescence decay with the slow decay lifetime τ_2 of 120.65 ns compared with that of 75.83 ns for the control film; this difference attested the significantly suppressed non-radiative recombination initiated by trap states on the perovskite surface. This phenomenon resulted in an enriched perovskite film and reduced grain boundary defects due to EACl-2.5% doping. The PL intensity was mapped to further investigate the impact of EACl on the optical dynamics of the thin film as given in Fig. 4c, d [41]. PL measurements provide direct insight into the non-radiative excitons' decay performance. The control film showed non-uniform peak intensity triggered by large trap flux, which contributed to poor carrier mobility [42,43]. Meanwhile, the EACl-2.5% film exhibited uniform and high peak intensity, suggesting a minimized non-radiative exciton decay, which was almost an order of magnitude higher than that of the EACl-0% film.

Fig. 5a shows the layered configuration of the final meso-structured device (glass/FTO/c-TiO_2/meso-TiO_2/perovskite/hole transporting layer (HTL)/Au) in this work. The paste of TiO_2 nanoparticles was synthesized as mentioned in our previous work [42], and it could form

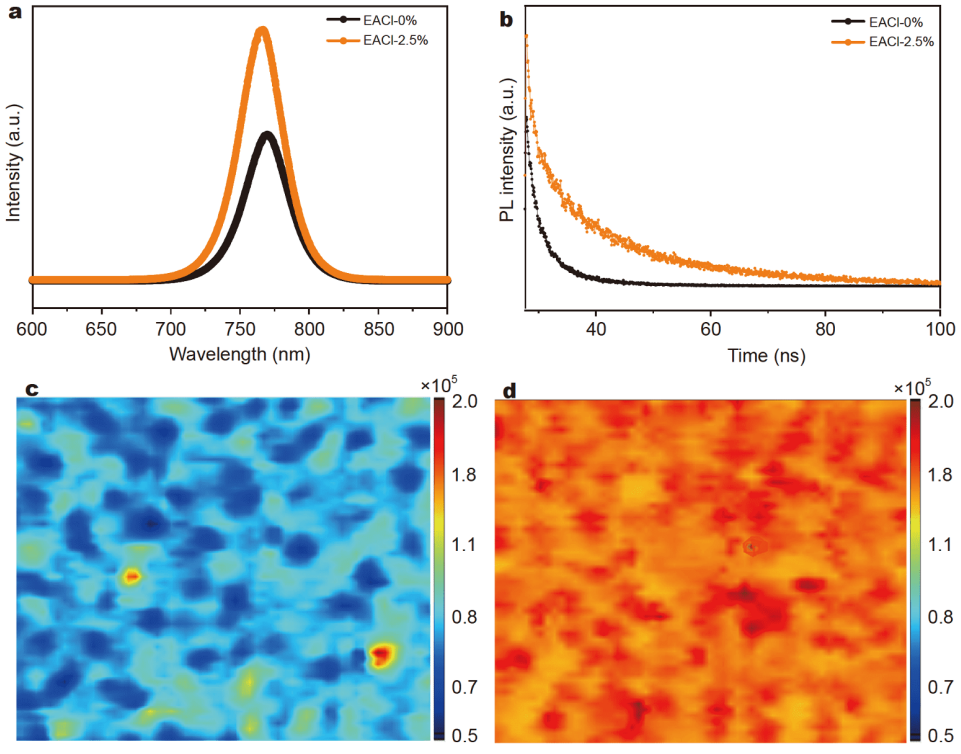

Figure 4 (a) Steady-state PL spectra of the EACl-0% and EACl-2.5% additive films. (b) TRPL spectra of the EACl-0% and EACl-2.5% films. PL intensity images from 740 to 790 nm for the (c) EACl-0% film and (d) EACl-2.5% additive film deposited on glass side.

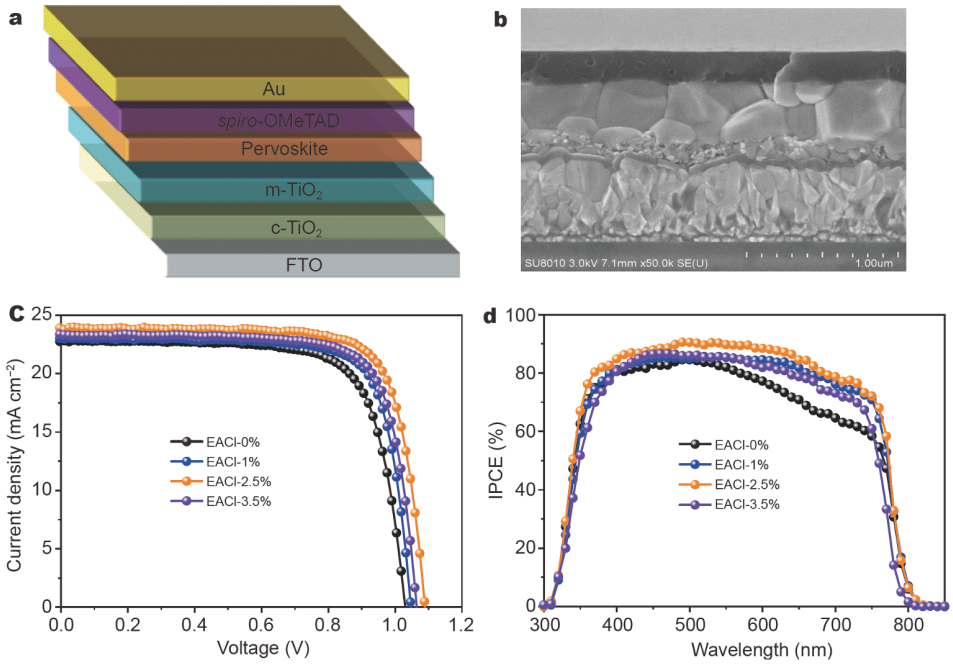

Figure 5 (a) Schematic layered configuration of the prepared EACl-2.5% device. (b) Cross-sectional SEM image of the final mesostructured device. (c) PCE curves, and (d) IPCE spectra of the respective prepared devices based on the perovskite films engineered with different concentrations of EACl.

an ultra-thin and electron collection-efficient mesoporous layer. The cross-sectional SEM image of the final device is presented in Fig. 5b. The underlying substrate was homogenously covered by the continuous and vertically grown large-grain perovskite active layer, which enabled charge carrier transport from a single crystal without the need of crossing grain boundaries. The performance characteristic was assessed by measuring the photocurrent density *versus* voltage. The effect of EACl additive engineering is remarkable in comparison with the conventional process (Fig. 5c). The detailed current density-voltage (*J-V*) parameters are briefed in Table 1.

Fill factor (FF; in %) and open-circuit voltage (V_{OC}) of the devices based on the EACl additives were significantly enhanced, probably due to the remarkably suppressed charge recombination caused by reduced defect density. Subsequently, the PCE remarkably increased from 17.35% for the control device to 20.03% for the EACl-2.5%-doped device [39]. Interestingly, the device based on the EACl-2.5% absorber layer also showed a small hysteresis (7%) compared with its counterpart EACl-0% (18%, Fig. S4).

The incident photon-to-current efficiency (IPCE) spectrum of the corresponding cell revealed high quantum yields over a wide spectrum ranging from 300 to 850 nm (Fig. 5d). The EACl-engineered film-based devices exhibited a broad reaction spectrum, particularly for EACl-2.5%.

The physical and chemical changes could have affected the performances of the PSCs. These changes could be due to different historical processes in the measurements [44]. The high IPCE values of the PSCs were credited to the strong and high absorption of UV-Vis light by the EACl-2.5% film and its effective electron-hole separation in the respective layers. The steady-state photocurrent

Table 1 *J-V* parameters of the best-performing PSCs based on the films with different amounts of EACl

Devices	J_{SC}[a] (mA cm^{-2})	V_{OC} (V)	FF (%)	PCE (%)
EACl-0%	22.35	1.03	73.01	17.35
EACl-1%	22.85	1.04	75.15	18.00
EACl-2.5%	23.51	1.08	76.99	20.03
EACl-3.5%	23.11	1.06	76.03	19.05

a) J_{SC} is short circuit current density.

output power of the devices based on the control and EACl-2.5% films was measured to affirm the power stability of 150 s at a bias of 0.9 V (Fig. S5). The fabrication of the devices from the EACl-2.5% process displayed a clearly stable power output compared with the control device.

The statistical distribution of PCEs for 32 individual control and EACl-2.5% engineered film-based devices is presented in Fig. 6a. The statistical constrictions of the EACl-2.5%-treated devices exhibited much finer spreading in the boosted efficiency region in comparison with the control devices. The EACl-2.5% devices presented high overall performance. Thus, the EACl-2.5% technique is an effective path to produce highly efficient and scalable mixed cation perovskite devices. Fig. 6b shows the photographs of contact angles for the EACl-0% and EACl-2.5% films, indicating the improvement in resistance against the humidity, which could probably help improve the stability against humidity.

The charge recombination and electric properties of the devices were studied *via* electrochemical impedance spectroscopy (EIS; Fig. 7a). The first semicircle of the EACl-0%-based cell was marginally smaller than that of EACl-2.5%, demonstrating that the EACl-0%-based cell had a considerably smaller charge transport resistance (R_{ct}) than EACl-2.5%. Series resistance was reduced by the enhanced crystallinity, while the shunt resistance increased by the diminished bulk and surface defects leading to an improved FF [45]. This phenomenon could be due to the considerably suppressed charge recombination caused by the reduced defect density.

The degradation of perovskite films is usually initialized at the defect sites of the film surface and grain boundaries, where the highly active and mobile molecules are highly vulnerable to oxygen and moisture. The aged stability of the control and EACl-2.5% devices was compared, and the normalized aged PCE results are presented in Fig. 7b. The PCE evolution of the un-encapsulated devices aged in a desiccator under 30% relative humidity for a period of 1000 h was assessed [46]. The EACL-0% device lost 60% of the initial PCE, while the EACl-2.5% device maintained around 89% of its initial efficiency during the same time period. This resilience of the stability could be due to several reasons. First, the intrinsic thermodynamic stability of the EACl-engineered layered structure allowed for strain relaxation and improved stability against the potential energy disorder. Second, the decreased defect sites at the surface and grain boundaries inhibited the permeation of oxygen and moisture through these defects.

The greatly reduced non-radiative recombination could be the cause of the noticeable enhancement in V_{OC}, as the majority of the V_{OC} losses in PSCs were proven to be affected by non-radiative recombination caused by surface charge traps. To verify this, a key method of transient photovoltage decay of PSCs was measured to probe the charge recombination and electron mobility process at the anode against the photospectral response under the open-circuit conditions (Fig. 7c). The photovoltage decay curve of the EACl-2.5% device showed a slow carrier time, thereby revealing a slow recombination rate of injected electrons. The carrier lifetime of the EACl-2.5%-based device was measured to be about five times higher than that of the EACl-0% based device, which supported the concept that charge carrier recombination throughout the entire device was suppressed in the EACl-2.5%-based cell [11,47,48]. The transient profile of V_{OC} for the cell based on the EACl-2.5%-additive film showed slow photovoltage decay. The electron lifetime was obtained using the following equation [49]:

$$\tau = -k_B T e^{-1} \left(dV_{OC} / dt \right)^{-1}, \quad (3)$$

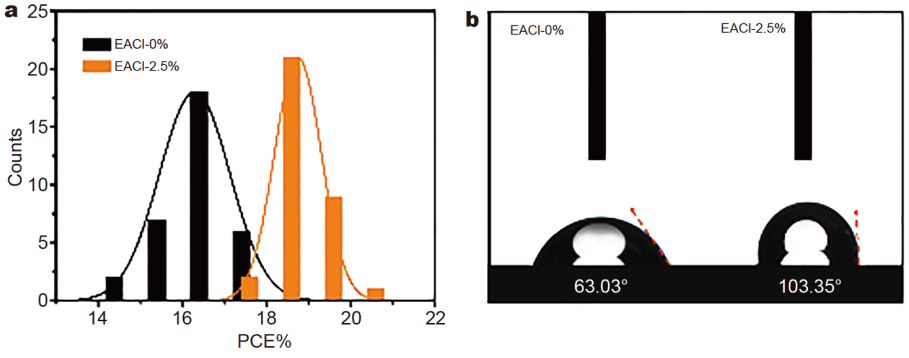

Figure 6 (a) Histogram of the PCE distribution for the devices based on the EACl-0% and EACl-2.5% perovskite absorber layers, which were calculated from 32 cells. (b) Static water contact angle measurements of the EACl-0% and EACl-2.5% films.

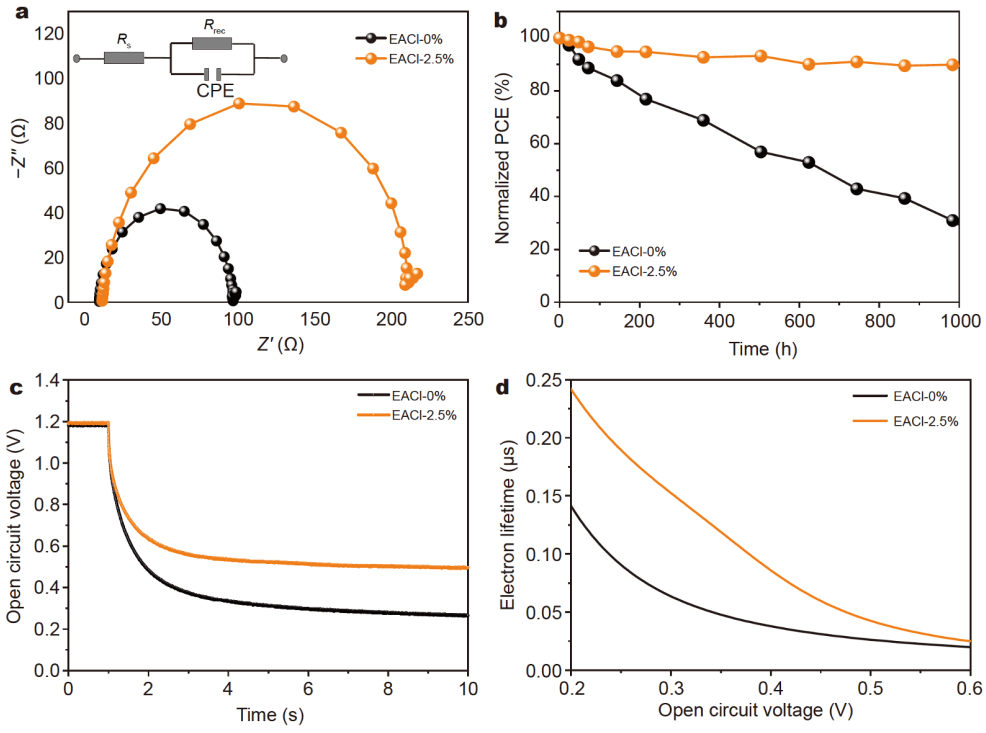

Figure 7 (a) EIS of the EACl-0%- and EACl-2.5%-based devices at a bias voltage of 0.90 V. (b) Normalized efficiency evolution of the devices aged for a period of 1000 h. (c)V_{OC} decay curves and (d) the correlation function between electron lifetime and V_{OC} of the EACl-0%- and EACl-2.5%-based devices.

where e is the elementary charge, T is the temperature, and k_B is the Boltzmann constant. The much-elongated electron lifetime under various voltages suggested carrier recombination throughout the entire device and proved that EACl processing efficiently reduced the trap state densities, resulting in the reduction of trap-assisted non-radiative and interfacial recombination, which was attributed to the increase in V_{OC}.

The electron lifetime increased as the addition of EACl in the treatment solution reached 2.5%, and this finding resulted from the improvement in the perovskite crystallinity and morphology (Fig. 7d) [50]. The EACl-2.5%-treated film showed a longer electron lifetime than the film without EACl-2.5% additive over the same voltage region. Carrier recombination throughout the entire device was suppressed in the former device, indicating that the cell with the EACl-2.5% film had a much lower interface recombination than that without the film. The EACl film effectively passivated the perovskite interface and hole transport across the film, thereby reducing interface recombination. The high-quality film was obtained with the fast charge transport method, which helped navigate the photocarrier from the perovskite layer into HTL and electron transporting layer (ETL). This novel work endorses the future potential of the introduced EACl-2.5%-induced additive engineering mechanism, which will further help researchers achieve high-performance and phase-resilient perovskite-based devices at the industrial scale.

CONCLUSION

In summary, a novel and facile reproducible approach based on EACl additive engineering was successfully introduced to fabricate perovskite films with superior uniformity, large grain size, excellent crystal quality, and few defects. The distinctive role of EACl in enhancing the perovskite film quality was revealed. EACl was found to promote perovskite crystal growth by forming a stable intermediate phase, and it was demonstrated to deplete during the annealing stage and evoked perovskite grain growth. The films obtained with EACl-2.5% as a doping agent exhibited large grains, dramatically reduced grain boundaries, extended charge carrier lifetimes, and significantly decreased defect densities without compromising the perovskite bandgap. Lastly, an effective PCE of 20.03% was achieved *via* adding EACl-2.5%, and the high-efficiency device could maintain over 89% of the initial PCE after aging for 1000 h at room temperature.

Received 27 March 2020; accepted 5 May 2020; published online 20 July 2020

1 Kojima A, Teshima K, Shirai Y, *et al.* Organometal halide perovskites as visible-light sensitizers for photovoltaic cells. J Am Chem Soc, 2009, 131: 6050–6051
2 Jung HS, Park NG. Perovskite solar cells: from materials to devices. Small, 2015, 11: 10–25
3 Jeon NJ, Noh JH, Yang WS, *et al.* Compositional engineering of perovskite materials for high-performance solar cells. Nature, 2015, 517: 476–480
4 Kim HS, Mora-Sero I, Gonzalez-Pedro V, *et al.* Mechanism of carrier accumulation in perovskite thin-absorber solar cells. Nat Commun, 2013, 4: 2242
5 Ball JM, Lee MM, Hey A, *et al.* Low-temperature processed meso-superstructured to thin-film perovskite solar cells. Energy Environ Sci, 2013, 6: 1739–1743
6 Liu C, Yang Y, Ding Y, *et al.* High-efficiency and UV-stable planar perovskite solar cells using a low-temperature, solution-processed electron-transport layer. ChemSusChem, 2018, 11: 1232–1237
7 Jiang Q, Zhao Y, Zhang X, *et al.* Surface passivation of perovskite film for efficient solar cells. Nat Photonics, 2019, 13: 460–466
8 https://www.nrel.gov/pv/assets/images/efficiency-\chart.png (accessed: 2019)
9 Guo L, Fei C, Zhang R, *et al.* Impact of sol aging on TiO_2 compact layer and photovoltaic performance of perovskite solar cell. Sci China Mater, 2016, 59: 710–718
10 Arain Z, Liu C, Ren Y, *et al.* Low-temperature annealed perovskite films: A trade-off between fast and retarded crystallization *via* solvent engineering. ACS Appl Mater Interfaces, 2019, 11: 16704–16712
11 Yang Y, Peng H, Liu C, *et al.* Bi-functional additive engineering for high-performance perovskite solar cells with reduced trap density. J Mater Chem A, 2019, 7: 6450–6458
12 Liang PW, Liao CY, Chueh CC, *et al.* Additive enhanced crystallization of solution-processed perovskite for highly efficient planar-heterojunction solar cells. Adv Mater, 2014, 26: 3748–3754
13 Chen J, Xu J, Xiao L, *et al.* Mixed-organic-cation $(FA)_x(MA)_{1-x}PbI_3$ planar perovskite solar cells with 16.48% efficiency *via* a low-pressure vapor-assisted solution process. ACS Appl Mater Interfaces, 2017, 9: 2449–2458
14 Wu YZ, Ding Y, Hayat T, *et al.* Enlarged working potential window for MnO_2 supercapacitors with neutral aqueous electrolytes. Appl Surf Sci, 2018, 459: 430–437
15 Dong Q, Fang Y, Shao Y, *et al.* Electron-hole diffusion lengths >175 μm in solution-grown $CH_3NH_3PbI_3$ single crystals. Science, 2015, 347: 967–970
16 Liu D, Gangishetty MK, Kelly TL. Effect of $CH_3NH_3PbI_3$ thickness on device efficiency in planar heterojunction perovskite solar cells. J Mater Chem A, 2014, 2: 19873–19881
17 Etgar L, Gao P, Xue Z, *et al.* Mesoscopic $CH_3NH_3PbI_3/TiO_2$ heterojunction solar cells. J Am Chem Soc, 2012, 134: 17396–17399
18 Zhang F, Cong J, Li Y, *et al.* A facile route to grain morphology controllable perovskite thin films towards highly efficient perovskite solar cells. Nano Energy, 2018, 53: 405–414
19 Bi D, Yi C, Luo J, *et al.* Polymer-templated nucleation and crystal growth of perovskite films for solar cells with efficiency greater than 21%. Nat Energy, 2016, 1: 16142
20 Zheng H, Dai S, Zhou K, *et al.* New-type highly stable 2D/3D perovskite materials: The effect of introducing ammonium cation on performance of perovskite solar cells. Sci China Mater, 2019, 62: 508–518
21 Ran C, Xu J, Gao W, *et al.* Defects in metal triiodide perovskite materials towards high-performance solar cells: origin, impact, characterization, and engineering. Chem Soc Rev, 2018, 47: 4581–4610
22 Jeon NJ, Noh JH, Kim YC, *et al.* Solvent engineering for high-performance inorganic–organic hybrid perovskite solar cells. Nat Mater, 2014, 13: 897–903
23 Ding X, Ren Y, Wu Y, *et al.* Sequential deposition method fabricating carbonbased fully-inorganic perovskite solar cells. Sci China Mater, 2018, 61: 73–79
24 Wu Y, Xie F, Chen H, *et al.* Thermally stable $MAPbI_3$ perovskite solar cells with efficiency of 19.19% and area over 1 cm^2 achieved by additive engineering. Adv Mater, 2017, 29: 1701073
25 Ma S, Cai M, Cheng T, *et al.* Two-dimensional organic-inorganic hybrid perovskite: From material properties to device applications. Sci China Mater, 2018, 61: 1257–1277
26 Wu CG, Chiang CH, Han HC. Manipulating the horizontal morphology and vertical distribution of the active layer in BHJ-PSC with a multi-functional solid organic additive. J Mater Chem A, 2014, 2: 5295–5303
27 Li X, Bi D, Yi C, *et al.* A vacuum flash-assisted solution process for high-efficiency large-area perovskite solar cells. Science, 2016, 353: 58–62
28 Arain Z, Liu C, Yang Y, *et al.* Elucidating the dynamics of solvent engineering for perovskite solar cells. Sci China Mater, 2019, 62: 161–172
29 Ahn N, Son DY, Jang IH, *et al.* Highly reproducible perovskite solar cells with average efficiency of 18.3% and best efficiency of 19.7% fabricated *via* Lewis base adduct of lead(II) iodide. J Am Chem Soc, 2015, 137: 8696–8699
30 Xu J, Buin A, Ip AH, *et al.* Perovskite-fullerene hybrid materials suppress hysteresis in planar diodes. Nat Commun, 2015, 6: 7081
31 Lee JW, Kim HS, Park NG. Lewis acid-base adduct approach for high efficiency perovskite solar cells. Acc Chem Res, 2016, 49: 311–319
32 Wu CG, Chiang CH, Tseng ZL, *et al.* High efficiency stable inverted perovskite solar cells without current hysteresis. Energy Environ Sci, 2015, 8: 2725–2733
33 Yin WJ, Chen H, Shi T, *et al.* Origin of high electronic quality in structurally disordered $CH_3NH_3PbI_3$ and the passivation effect of Cl and O at grain boundaries. Adv Electron Mater, 2015, 1: 1500044
34 Mateen M, Arain Z, Yang Y, *et al.* MACl-induced intermediate engineering for high-performance mixed-cation perovskite solar cells. ACS Appl Mater Interfaces, 2020, 12: 10535–10543
35 Dong Q, Yuan Y, Shao Y, *et al.* Abnormal crystal growth in $CH_3NH_3PbI_{3-x}Cl_x$ using a multi-cycle solution coating process. Energy Environ Sci, 2015, 8: 2464–2470
36 Xie F, Chen CC, Wu Y, *et al.* Vertical recrystallization for highly efficient and stable formamidinium-based inverted-structure perovskite solar cells. Energy Environ Sci, 2017, 10: 1942–1949
37 Mateen M, Arain Z, Liu C, *et al.* High-quality $(FA)_x(MA)_{1-x}PbI_3$ for efficient perovskite solar cells *via* a facile cation-intermixing technique. ACS Sustain Chem Eng, 2019, 7: 11760–11768
38 Ren Y, Duan B, Xu Y, *et al.* New insight into solvent engineering technology from evolution of intermediates *via* one-step spin-coating approach. Sci China Mater, 2017, 60: 392–398
39 Mateen M, Arain Z, Liu X, *et al.* High-performance mixed-cation

mixed-halide perovskite solar cells enabled by a facile intermediate engineering technique. J Power Sources, 2019, 448: 227386
40 Zhao W, Yang D, Liu SF. Organic-inorganic hybrid perovskite with controlled dopant modification and application in photovoltaic device. Small, 2017, 13: 1604153
41 Ren Y, Hao Y, Zhang N, *et al.* Exploration of polymer-assisted crystallization kinetics in $CsPbBr_3$ all-inorganic solar cell. Chem Eng J, 2019, 392: 123805
42 Handa T, Tex DM, Shimazaki A, *et al.* Charge injection mechanism at heterointerfaces in $CH_3NH_3PbI_3$ perovskite solar cells revealed by simultaneous time-resolved photoluminescence and photocurrent measurements. J Phys Chem Lett, 2017, 8: 954–960
43 Shi P, Ding Y, Liu C, *et al.* Advanced partial nucleation for single-phase $FA_{0.92}MA_{0.08}PbI_3$-based high-efficiency perovskite solar cells. Sci China Mater, 2019, 62: 1846–1856
44 Zhou Z, Xu J, Xiao L, *et al.* Efficient planar perovskite solar cells prepared *via* a low-pressure vapor-assisted solution process with fullerene/TiO_2 as an electron collection bilayer. RSC Adv, 2016, 6: 78585–78594
45 Wu YH, Ding Y, Liu XY, *et al.* Ambient stable $FAPbI_3$-based perovskite solar cells with a 2D-$EDAPbI_4$ thin capping layer. Sci China Mater, 2019, 63: 47–54
46 Sajid S, Elseman AM, Wei D, *et al.* NiO@carbon spheres: A promising composite electrode for scalable fabrication of planar perovskite solar cells at low cost. Nano Energy, 2019, 55: 470–476
47 Ma S, Qiao W, Cheng T, *et al.* Optical-electrical-chemical engineering of PEDOT:PSS by incorporation of hydrophobic nafion for efficient and stable perovskite solar cells. ACS Appl Mater Interfaces, 2018, 10: 3902–3911
48 Zhang X, Zhou Z', Ma S, *et al.* Fused tetraphenylethylene-triphenylamine as an efficient hole transporting material in perovskite solar cells. Chem Commun, 2020, 56: 3159–3162
49 Wang Z, Wang L. Photoelectrode for water splitting: Materials, fabrication and characterization. Sci China Mater, 2018, 61: 806–821
50 Sun M, Zhang F, Liu H, *et al.* Tuning the crystal growth of perovskite thin-films by adding the 2-pyridylthiourea additive for highly efficient and stable solar cells prepared in ambient air. J Mater Chem A, 2017, 5: 13448–13456

Acknowledgements This work was supported by the National Key R&D Program of China (2019YFB1503202), the 111 Project (B16016), the National Natural Science Foundation of China (51702096, U1705256 and 61904053), and the Fundamental Research Funds for the Central Universities (2019MS026, 2019MS027 and 2020MS080).

Author contributions Mateen M performed the main experiments and wrote the paper; Ren Y, Zhang X, Iqbal A, Liu C, Chen Q, Ma S, and Cai M helped to fabricate the devices, analyze the data; Arain Z, Liu X and Ding Y helped to conceive the framework of this paper and review the manuscript; Dai S supervised the project. All authors contributed to the general discussion about the work.

Conflict of interest The authors declare that they have no conflict of interest.

Supplementary information Experimental details and supporting data are available in the online version of the paper.

Muhammad Mateen obtained his Master's degree from the Shah Abdul Latif University. Currently, he is a PhD candidate in North China Electric Power University (NCEPU) under the supervision of Prof. Songyuan Dai. His research interests mainly focus on the perovskite solar cells.

Xuepeng Liu received his PhD from the University of Science and Technology of China (USTC) in 2018. He is a lecture in NCEPU now. His research interests focus on perovskite solar cells.

Yong Ding received his PhD degree from Hefei Institutes of Physical Science, Chinese Academy of Sciences (CAS) in 2016. After graduation, he became a lecturer in NCEPU. His research interests focus on the 2D perovskite-based photoelectric devices, including perovskite solar cells and light-emitting diodes.

Songyuan Dai is a professor in NCEPU. He obtained his BSc degree in physics from Anhui Normal University in 1987, and MSc and PhD degrees in plasma physics from the Institute of Plasma Physics, Chinese Academy of Sciences in 1991 and 2001, respectively. His research interests mainly focus on the next-generation solar cells including dye-sensitized solar cells, quantum dot solar cells and perovskite solar cells.

通过乙胺盐酸盐添加剂工程提升$MAPbI_3$钙钛矿太阳电池的光电性能

Muhammad Mateen[1], Zulqarnain Arain[1,3], 刘雪朋[1*], Atif Iqbal[1], 任英科[4], 张先付[1], 刘成[1], 陈钦[1], 马爽[1], 丁勇[1,2*], 蔡墨朗[1,2], 戴松元[1,2*]

摘要 钙钛矿光吸收层的质量对太阳电池的光伏性能有重要的影响. 目前, 制备甲基铵基碘化铅钙钛矿($MAPbI_3$)的方法会产生大量缺陷态, 特别是在晶界和薄膜表面, 这些问题阻碍了钙钛矿太阳电池性能进一步提升. 本文介绍了一种采用乙胺盐酸盐(EACl)添加剂制备高质量$MAPbI_3$的特殊方法, 发现EACl可以使得钙钛矿晶体不通过中间相形成, 并在退火后从钙钛矿中蒸发. 此外, 该方法还获得了梯度钙钛矿结构, 显著提高了钙钛矿薄膜的性能. 在最佳EACl用量下, 器件的光电转换效率(PCE)达到20.03%. 器件在室温老化1000 h后仍能保持原有PCE的89%. 这一新方法可以简易制备高质量、缺陷少的钙钛矿薄膜, 以生产更加稳定的器件.

